ACS APPLIED MATERIALS & INTERFACES

Research Article

www.acsami.org

Amphiphilic Gold Nanoparticles Displaying Flexible Bifurcated Ligands as a Carrier for siRNA Delivery into the Cell Cytosol

Kenichi Niikura,*[,†,‡] Kenya Kobayashi,[†,§] Chie Takeuchi,[‡] Naoki Fujitani,[‡] Shuko Takahara,[‡] Takafumi Ninomiya,[⊥] Kyoji Hagiwara,[§] Hideyuki Mitomo,[‡] Yoshihiro Ito,[§] Yoshihito Osada,[§] and Kuniharu Ijiro*[,‡]

[‡]Research Institute for Electronic Science (RIES), Hokkaido University, Kita 21, Nishi 10, Kita-ku, Sapporo, Hokkaido 001-0021, Japan

[§]Nano Medical Engineering Laboratory, RIKEN, 2-1, Hirosawa, Wako, Saitama 351-0198, Japan

[⊥]Department of Anatomy 1, Sapporo Medical University School of Medicine, West 17, South 1, Chuo-ku, Sapporo, Hokkaido 060-8556, Japan

Supporting Information

ABSTRACT: The nanoparticle-based delivery of siRNA with a noncationic outermost surface at a low particle concentration is greatly desired. We newly synthesized a bifurcated ligand (BL) possessing hydrophobic and hydrophilic arms as a surface ligand for gold nanoparticles (AuNPs) to allow siRNA delivery. The concept underlying the design of this ligand is that amphiphilic property should allow AuNPs to permeate the cell cytosol thorough the endosomal membrane. BLs and quaternary cationic ligands were codisplayed on 40 nm AuNPs, which were subsequently coated with siRNA via electrostatic interaction. The number of siRNAs immobilized on a single nanoparticle was 26, and the conjugate showed a negative zeta potential due to siRNAs on the outermost surface of the AuNPs. Apparent gene silencing of luciferase expression in HeLa cells was achieved at an AuNP concentration as low as 60 pM. Almost no gene silencing was observed for AuNPs not displaying BLs. To reveal the effect of the BL, we compared the number of AuNPs internalized into HeLa cells and the localization in the cytosol between AuNPs displaying and those not displaying BLs. These analyses indicated that the role of BLs is not only the simple promotion of cellular uptake but also involves the enhancement of AuNPs permeation into the cytosol from the endosomes, leading to effective gene silencing.

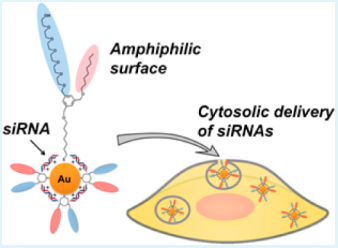

KEYWORDS: *siRNA delivery, gold nanoparticles, bifurcated ligands, amphiphilic nanoparticle, endosome escape*

INTRODUCTION

Short-length RNAs, such as small interfering RNA (siRNA) and microRNA (miRNA), are considered to be strong candidates in the development of next-generation nucleic acid medicines with the potential for the tailor-made therapy for various types of diseases.[1−6] Although they are of biological interests, the application of siRNAs requires the development of carrier devices due to their low cellular membrane permeability and ready degradability. In the past decade, therefore, carrier molecules have been developed for the delivery of siRNA into target cells and cancer tissues.[7,8] Among the various types of siRNA carriers developed to date, gold nanoparticles (AuNPs)[9−14] are one of the most attractive devices because of their biocompatibility[15] and the potential to accurately control their size.[16] In fact, several types of siRNA-AuNP conjugates have already been developed. Nagasaki et al. reported that the codisplay of thiolated siRNAs and PEG-*block*-poly(2-(N,N-dimethylamino)ethyl methacrylate) polymer on 15 nm AuNPs induced gene silencing at AuNPs with concentrations ranging from 50 to 100 nM.[17] Mirkin et al. also reported that AuNPs with a diameter ∼13 nm displaying multivalent siRNAs could induce gene silencing.[18] To apply these techniques to effective gene silencing, thiolated siRNAs are required for the construction of covalent Au−S bonds as well as the introduction of a spacer structure[19] to provide a release mechanism for the siRNA into the cytosol.

As an alternative method, a layer-by-layer (LbL) approach that eliminates the need for thiolated siRNA has been proposed. This approach is based on the electrostatic interaction between a positively charged polymer such as polyethylenimine (PEI), and negatively charged siRNAs.[20,21] Goepferich et al. reported that the knockdown of green fluorescent protein (GFP) expression was observed only when the outermost layer of AuNPs was composed of a PEI, although this activity was not found in the case of siRNA alone without an outermost PEI layer.[22] On the other hand, it has been reported that cationic nanoparticles sometimes showed cytotoxicity.[23−26] Therefore, there is a great demand for the development of an improved and viable AuNP-based siRNA-delivery system that can eliminate cytotoxicity and allow further therapeutic applications.

Received: August 19, 2014
Accepted: December 3, 2014
Published: December 3, 2014

Increased cellular uptake efficiency is another important issue behind the development of AuNPs-based siRNA carrier. The display of amphiphilic surface ligands is speculated to aid in increasing uptake efficiency. Some amphiphilic nanoparticles have been proposed to date. Eychmüller et al. reported that methoxypolyethylene glycol [CH_3-$(OCH_2CH_2)_7$-SH]-coated CdTe nanocrystals (several nm in a diameter) acquired a characteristic property allowing triphase transfer from toluene through water into chloroform.[27,28]

We have previously demonstrated that thiolated-PEG ligands with a terminus consisting of a short alkyl chain provide AuNPs (10 nm in a diameter) with an amphiphilic property and facilitate the phase transfer of AuNPs from aqueous to organic solvents.[29,30] Stellacci et al. demonstrated that AuNPs (4.5 nm in diameter) coated with both hydrophobic ligands and anionic ligands in a striped fashion could penetrate the cellular membrane of DC2.4 cells.[31] Zubarev et al. reported that AuNPs (2 nm in a diameter) covered with a V-shaped diblock polymer consisting of hydrophilic PEG and hydrophobic polybutadiene arms (M_w = 7100), enabled the AuNPs to be dissolved in seven kinds of conventional solvents, including polar and nonpolar solvents, with long-term stability (over 2 years).[32] Inspired by Zubarev's design, we designed a bifurcated surface ligand of smaller molecular size.

Further, to ensure the expression of siRNA activity, the AuNP carrier must allow the cytosolic delivery of siRNA. Previously reported carriers often comprised an amine-containing polymer, such as PEI,[33−36] or cell-penetrating peptides[37] aimed at ensuring their endosomal escape or direct membrane penetration. We, however, speculated that the amphiphilic property of nanoparticles would enable the efficient siRNA delivery into cells through the hydrophobic cellular membrane.

In this study, we designed and synthesized a bifurcated surface ligand (BL) with a structure consisting of two short hexaethylene glycol (hydrophilic) and octyl ether (hydrophobic) arms (Scheme 1), aiming to facilitate transport of siRNA across the endosomal membrane. As these two arms are linked via a flexible ether bond, the AuNPs are expected to adapt to both polar and nonpolar solutions through the rotation of the hydrophilic/hydrophobic arms to minimalize their surface energy. To immobilize siRNA on AuNPs via electrostatic interactions, we codisplayed a quaternary ammonium ligand, (16-mercaptohexadecyl) trimethylammonium bromide (MTAB),[38] with the BL to allow siRNAs to be gradually released within the cell. We here present the effects of the AuNP-displayed BL molecules on the knockdown efficiency of the luciferase gene in HeLa cells in comparison to AuNPs displaying MTAB alone.

Scheme 1. Thiolated Ligands Used in This Work

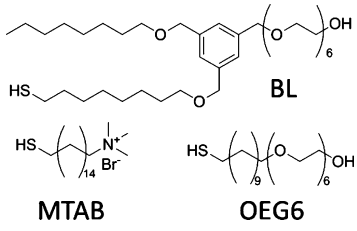

RESULTS AND DISCUSSION

Syntheses of BLs. BLs were successfully synthesized from 1,3,5-Tris(bromomethyl)benzene in five steps according to Scheme S1 in the Supporting Information. To this starting material, we introduced *n*-octanol, 7-octene-1-ol, and hexaethylene glycol in a stepwise manner via ether linkages. Successive radical addition of thioacetic acid to the olefin moiety and subsequent hydrolysis of the thioacetate moiety produced the desired BLs as a pale yellow syrup (5% in 5 steps).

Characterization of BL-displayed AuNPs. The amphiphilic property of the surface of the BL-modified AuNPs (BL-AuNPs) was investigated by examination of the phase transfer behavior from an aqueous to an organic layer (see Materials and Methods for details of the protocol) and the differences in the mobility of hydrophilic and hydrophobic arms of the BL on AuNPs were analyzed by NMR experiments under both hydrophilic and hydrophobic conditions. To investigate the phase transfer behavior, we prepared 10 nm of BL-AuNPs and OEG6-modified AuNPs (OEG6-AuNPs) without hydrophobic arms (as a control of hydrophilic AuNPs) in water, and then chloroform was added as the organic layer (Figure 1a). After vigorous mixing, only BL-AuNPs were transferred from the aqueous to the organic phase, with the OEG6-AuNPs predominantly found in the aqueous layer or accumulated at the interface as shown in Figure 1b. This result revealed that BL-AuNPs could pass the interface between the hydrophilic and hydrophobic phase. The fact that OEG6-AuNPs could not shift to the organic layer suggested that the hydrophobic arm of the BL greatly contributes to the ability to cross the interface and disperse into an organic environment. In general, it is difficult for OEG6-coated nanoparticles to transfer from an aqueous phase to a hydrophobic phase because of their hydrophilicity, which suggests that it is difficult for them to cross the cell membrane. However, BL-displaying AuNPs could shift from an aqueous to a hydrophilic layer, as shown in Figure 1, despite the fact that the BL also contains an OEG6 moiety. This indicates that the structural features of BL, which contains both an alkyl chain and OEG6 to provide adequate hydrophobicity and hydrophilicity, might effectively contribute to its interaction with the hydrophobic layer and permit phase transfer. Therefore, inclusion of BLs in the AuNPs coating is expected to increase affinity to plasma and endosomal membranes, thereby leading to an increase in cellular uptake and a greater opportunity for endosomal escape.

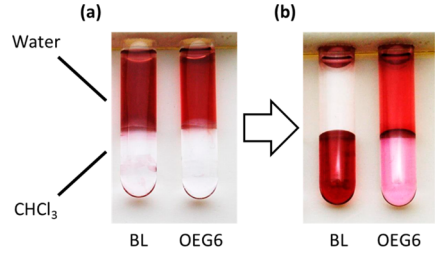

Figure 1. Phase transfer of AuNPs (10 nm in diameter). (a) before and (b) after vigorous mixing (left, BL-AuNPs; right, OEG6-AuNPs).

NMR spectroscopy is one of the most commonly used techniques for the investigation of ligand structures on AuNPs, although a high degree of line-broadening is known to occur because of the very short relaxation time of AuNPs. Recently,

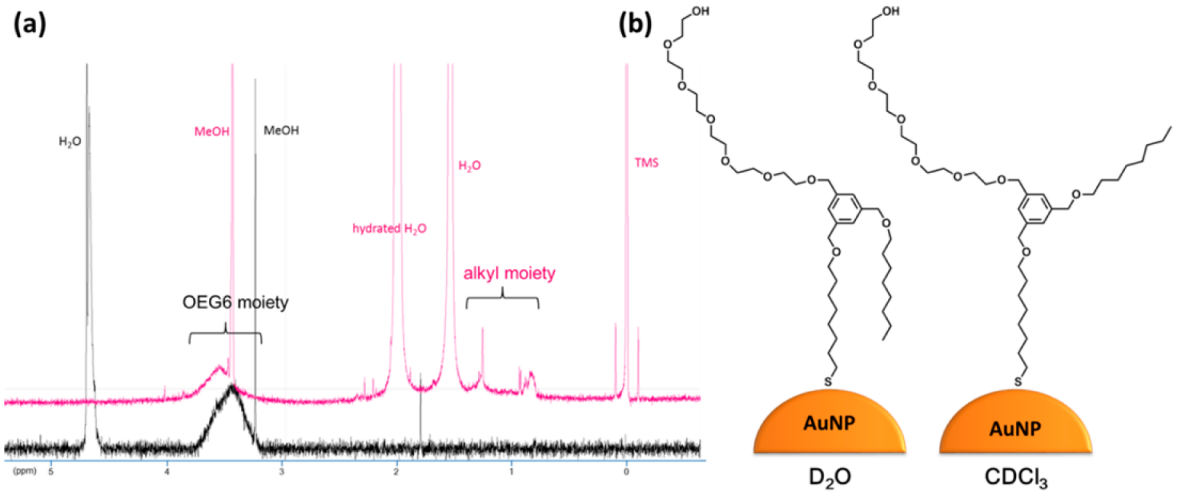

Figure 2. (a) ^{1}H NMR spectra of BL-AuNPs (10 nm) in D_2O (black) and in $CDCl_3$ (magenta). (b) Conformation of BLs on AuNPs in D_2O and $CDCl_3$ speculated from NMR.

NMR studies of AuNPs have been used in the determination of ligand-shell morphology, such as Janus or random conformations,[39,40] and ligand mobility on AuNP surfaces.[29] Here we measured the ^{1}H NMR spectra of BL-AuNPs dispersed in D_2O and $CDCl_3$ to clarify differences in the motion of BLs on the AuNP surface under hydrophilic and hydrophobic conditions. Prior to the NMR experiments, the residual free ligands were carefully removed by centrifugation as described in Material and Methods. Characteristically, the NMR spectrum of BL-AuNPs in D_2O showed that the signals derived from the alkyl chain had been abolished due to significant line-broadening, although the broadened OEG6 protons could be detected at around 3.2 ppm as shown in Figure 2a. This suggested that the motion of the hydrophobic alkyl chain was significantly restricted in a hydrophilic solvent due to hydrophobic interactions between the alkyl moiety and the AuNP (Figure 2b). Additionally, the OEG6 arms showed high solvent accessibility and contributed to the dispersion of BL-AuNPs in water. On the other hand, in hydrophobic $CDCl_3$, the signals derived from both the alkyl and OEG6 moieties were observed on the NMR spectrum of BL-AuNPs, suggesting that the hydrophobic alkyl arms possess greater flexibility under hydrophobic than under hydrophilic conditions and that both arms demonstrate solvent accessibility in a hydrophobic solvent. The NMR spectrum in $CDCl_3$ also indicated the clear compatibility to water of BL-AuNPs. The observed signal at around 1.5 ppm (Figure 2a) was that of the residual solvent water. The signal found at 2.0 ppm is thought to represent hydrated water coupled with the BL-AuNPs, based on the evidence of the observation of coupling between the signal and water in COSY spectrum (see Figure S2 in the Supporting Information). The NMR experiments indicated that the alterations in the mobility of the alkyl chain in the amphiphilic BLs enabled the AuNPs to adapt to both hydrophilic and hydrophobic environments by the modulation of solvent accessibility.

Preparation of AuNPs Codisplaying BL and MTAB as a siRNA Carrier. We chose AuNPs of 40 nm in diameter for siRNA delivery based on the report of Chan et al. that stated that the cellular uptake of AuNPs was particularly size-sensitive, and that AuNPs with a diameter of ~50 nm were efficiently taken up into HeLa cells.[41] To load siRNAs onto the AuNPs via electrostatic interactions, we codisplayed a quaternary cationic ligand, MTAB, that was originally developed by Zubarev and co-workers as a stable surface ligand for gold nanorods[38] with BLs on the surface of the AuNPs (Figure 3). First, AuNPs with

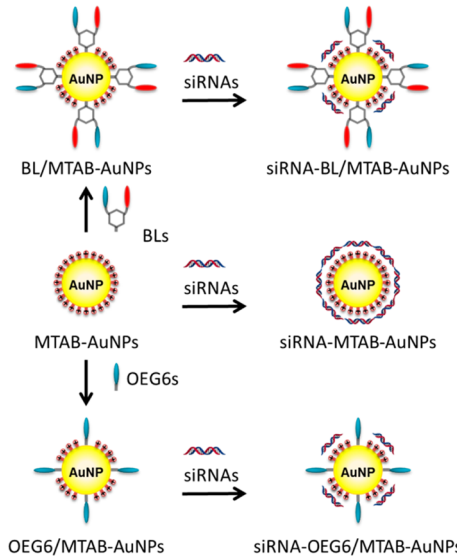

Figure 3. Flowchart for the preparation of siRNA-immobilized AuNPs.

a diameter of 40 nm were prepared according to Murphy's method in the presence of cetyltrimethylammonium bromide (CTAB) as a stabilizer.[42,43] After the as-synthesized AuNPs were washed, the remaining CTAB molecules were exchanged by the addition of a large excess of MTAB. The excess MTAB was thereafter removed by centrifugation and the concentration was adjusted to 1 nM AuNPs. Partial ligand exchange of MTABs to BLs was carried out by the addition of a methanolic solution of the BLs (Final concentration of BL was 1 mM) to an aqueous dispersion of MTAB-AuNPs, followed by incubation for 4 h at room temperature. The progress of the ligand exchange was confirmed by the detection of the zeta potential change of the AuNPs. After exposure to BLs for 4 h, the zeta potential was altered from +69.8 mV to +55.5 mV (Δ of zeta potential was found to be 14.3 mV), indicating that approximately 20% of the MTABs were exchanged for BLs. When the incubation time was extended to 24 h, the zeta

potential approached to +16.5 mV, suggesting an increase in the amount of BL incorporated.

In a similar fashion, the partial exchange of MTABs to OEG6s was also achieved, as confirmed by the alteration in zeta potential from +69.8 mV to +57.3 mV (Δ of zeta potential was found to be 12.5 mV).

After excess BLs were removed by centrifugation, double-stranded 21 mer siRNAs were added to an aqueous dispersion of MTAB-AuNPs or BL- and MTAB-*co*-displayed AuNPs (BL/MTAB-AuNPs) at a final concentration of 2.5 μM and incubated for 3 h. The inversion of the zeta potential from positive to negative values and a slight increase in diameter as measured by the dynamic light scattering (DLS) method were observed for both AuNPs (Figure 4). The zeta potential and

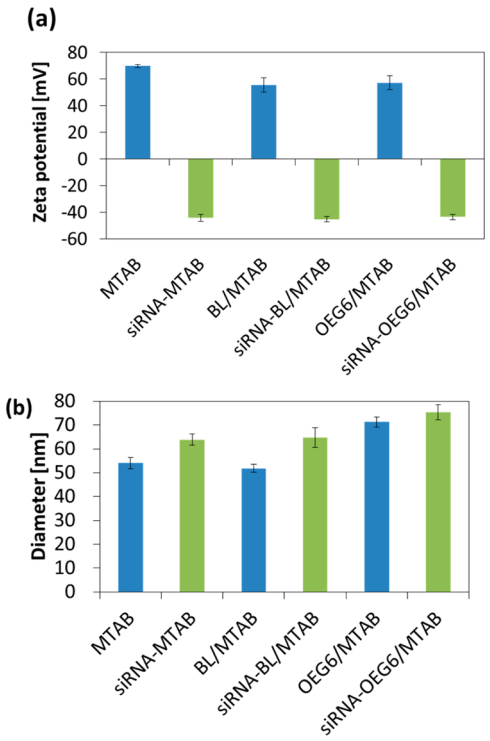

Figure 4. Characterization of AuNPs (40 nm in diameter). Before (blue) and after (green) immobilization of siRNA. (a): Zeta potentials of AuNPs. (b): Hydrodynamic diameters of AuNPs measured by DLS using the cumulant method. Data and standard deviations were obtained from three runs.

diameter of MTAB-AuNPs were +69.8 mV and 54.3 nm, respectively, whereas the values were found to be −44.3 mV and 63.9 nm, respectively, after siRNA immobilization, indicating the successful binding of siRNAs maintaining a single dispersion state without AuNP aggregation. Similar trends were observed for BL/MTAB-AuNPs and OEG6/MTAB-AuNPs (see Figure 4a, b for the zeta potentials and diameters, respectively), which showed that the incorporation of siRNAs into both BL/MTAB-AuNPs and OEG6/MTAB-AuNPs was successfully achieved. The important thing to notice here is that the surface of the AuNPs after incubation with siRNAs was negatively charged. A negatively charged surface leads to the elimination of cytotoxicity and the nonspecific adsorption of various proteins observed for positively charged surface, and is advantageous to in vivo applications.

Measurement of the fluorescence intensity of Alexa Fluor 488-attached siRNA (see details in Materials and Methods) showed that the number of siRNA incorporated onto each AuNP was calculated to be 109 and 26 for MTAB-AuNPs and BL/MTAB-AuNPs, respectively. The number for BL/MTAB-AuNPs was smaller than that for MTAB-AuNPs, which corresponds to the fact that MTAB-AuNPs showed a higher zeta potential compared to the BL/MTAB-AuNPs (Figure 4a). The calculated number of siRNA incorporated onto a BL/MTAB-AuNP (26 siRNA/single NP) was notably smaller than the expected value (approximately 87). For 20% ligand exchange from MTAB to BL, the number of incorporated siRNA onto a single AuNP is speculated to be about 87 if the relationship between cationic MTAB and anionic siRNA forms a linear correlation. Therefore, it is speculated that the relationship between BL/MTAB-AuNPs and siRNAs is a nonlinear correlation. The smaller-than-expected number of siRNAs bound to BL/MTAB-AuNPs might be attributed to the effect of steric hindrance derived from the biantennary structure of the BL, which includes both an OEG6 moiety and an alkyl chain. The OEG6 moiety, in particular, showed a greater flexibility in aqueous solution, according to the NMR study shown in Figure 2, thus blocking binding to siRNA. Nevertheless, we found that 26 siRNAs were sufficient to the silencing of gene expression, and BL/MTAB-AuNPs showed great potential as a transporter of siRNA to cellular cytosol as described below.

To investigate the potential use of AuNPs proposed here as a siRNA carrier, we performed the assays of the gene silencing using HeLa cells that stably express luciferase. Dose-dependent knockdown activity was examined for three types of complexes; siRNA-BL/MTAB-AuNPs, siRNA-MTAB-AuNPs, and siRNA-OEG6/MTAB-AuNPs as a negative control. The expression level of luciferase in cells after incubation with 60 pM siRNA-BL/MTAB-AuNPs was significantly reduced to approximately 44%, whereas incubation with siRNA-OEG6/MTAB-AuNPs and siRNA-MTAB-AuNPs resulted in only slight decreases to 92 and 95%, respectively, at the same AuNP concentration (Figure 5a). Note that the BL/MTAB-AuNPs showed the highest activity of all the AuNPs, while the siRNA-binding activity of the MTAB-AuNPs was higher than that of BL/MTAB-AuNPs. These data clearly indicate that BL molecules play a crucial role in effective gene silencing and thereby contribute to the passage of siRNA into cells. The low siRNA activity of siRNA-MTAB-AuNPs was consistent with the previous report by Goepferich et al. demonstrating that a siRNA-PEI-AuNP conjugate bearing an anionic surface layer of siRNA did not result in gene silencing.[22]

When nontargeted siRNAs were used, no gene silencing was observed for these three conjugations, indicating that the knockdown activity was induced in a sequence-specific manner instead of as an unexpected and nonspecific effect of the BL. In addition, it is important to note that previous reports of obvious gene silencing with an AuNP concentration as low as 60 pM were limited. Previous studies, such as Reich et al., have reported gene silencing of GFP in C166 cells in the presence of 10 pM of gold nanoshells as carrier with the aid of laser irradiation.[44] Goepferich et al. achieved gene knockdown of EGFP in CHO-K1 cells with 0.37 nM of AuNPs using an LbL approach.[22] Although direct comparison may be difficult due to differences in cell line and the targeted gene sequence used in each study, our method, based on anionic particles without any external assistance such as laser irradiation, appears to be the

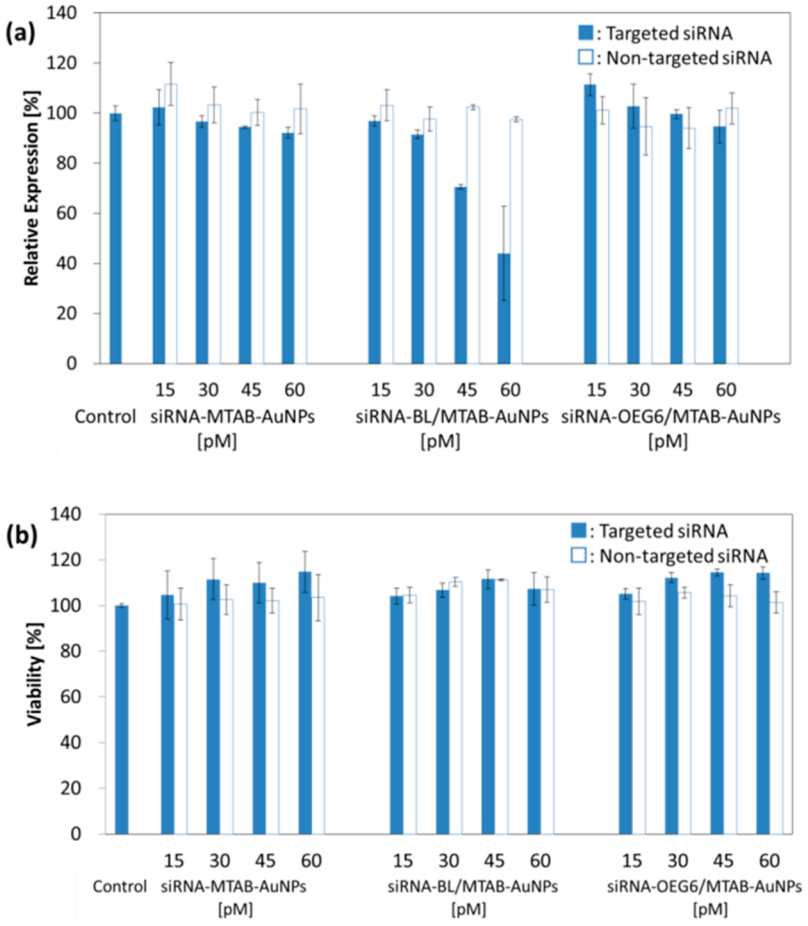

Figure 5. (a): Relative expression of luciferase in HeLa cells after incubation with AuNPs. (b): Cytotoxicity determined using the CCK-8 system. Blue, targeted siRNA; white, nontargeted siRNA. Control bar present no addition of siRNA-AuNPs. Concentrations are based on the AuNPs. Data and standard deviations were obtained from three different wells.

one of the most effective reported to date. Furthermore, this siRNA-BL/MTAB-AuNPs conjugate possesses a negatively charged surface, which is desirable for the avoidance of the nonspecific adsorption of various proteins as well as cytotoxicity. These two factors afford advantages for the future therapeutic applications. No obvious cytotoxicity to the HeLa cells was observed for the range of AuNP concentrations tested (Figure 5b).

Among the three types of AuNPs tested, only the BL/MTAB-AuNP-induced apparent knockdown activity. On basis of this fact, we speculated that the affinity of BL to the plasma or endosomal membranes might have contributed to the effective cellular uptake and further escape to the cytosol. Therefore, we investigated the number of AuNPs taken up into the cells as well as distribution of the AuNPs in cells. The average number of AuNPs taken up into an individual cell after incubation for 3 h was determined by inductively coupled plasma atomic emission spectroscopy (ICP-AES). The average number was revealed to be 280, 330, and 230 for siRNA-MTAB-, siRNA-BL/MTAB- and siRNA-OEG6/MTAB-AuNPs, respectively (Figure 6). Interestingly, there was a significant difference between siRNA-BL/MTAB- and siRNA-OEG6/MTAB-AuNPs (P = 0.018), suggesting that BL structure promoted a higher level of cellular uptake than that for just hydrophilic siRNA-OEG6/MTAB-AuNPs. In fact, the amphiphilic BL might be needed to allow easy access to cells and to confer higher affinity to the hydrophobic conditions

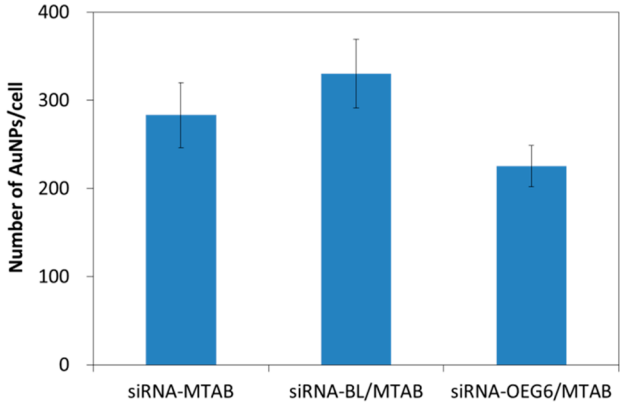

Figure 6. Number of AuNPs internalized into per HeLa cell determined with ICP. HeLa cells were incubated for 20 h in the presence of 30 pM of AuNPs. Data and standard deviations were obtained from three runs.

than that offered by the single OEG6 structure, a speculation that was supported by the results of the phase transfer experiment shown in Figure 1. However, the elucidation of the mechanism of cellular uptake; i.e., endocytosis or cell penetration, remains to be resolved.

On the other hand, there was no significant difference between the number of siRNA-BL/MTAB-AuNPs and siRNA-MTAB-AuNPs in each cell. The differences in the number of

AuNPs among the three types of AuNP were too small to conclude the existence of any effect on knockdown activity, implying that the role of BL is not simply an enhancement of the cellular uptake of AuNPs. We, therefore, explored their distribution of the three types of AuNP in cells.

Delivery of siRNAs to the cytosol is crucial to achieving effective knockdown activity.[45−47] The BL is assumed to have a role in enabling cellular membrane permeation or endosomal escape after cellular uptake via endocytosis, both of which lead to the translocation of the AuNPs within the cytosol. Figure 7

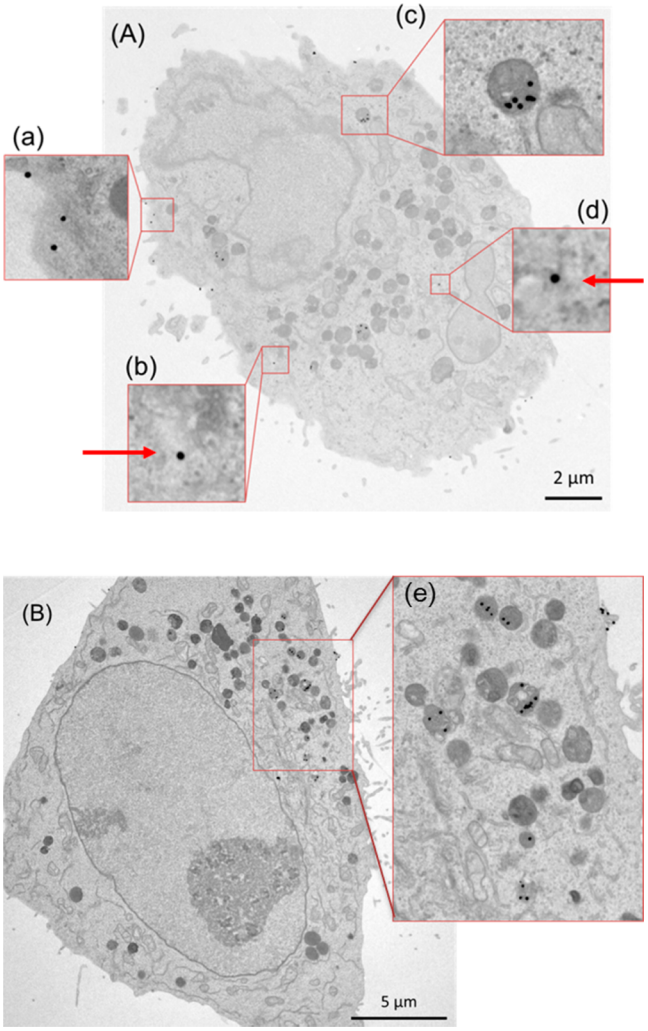

Figure 7. Ultrathin section image of HeLa cells observed by TEM. (A) TEM image of a HeLa cell after incubation with siRNA-BL/MTAB-AuNPs. (a)−(d) Representative enlarged figures derived from A. (B) After incubation with siRNA-MTAB-AuNPs. (e) Representative enlarged figures derived from B. Fixed with 2.5% glutaraldehyde. Red arrows indicate AuNPs within the cytosol.

shows representative transmission electron microscope (TEM) images of sectioned HeLa cells after incubation with AuNPs for 3 h. Figure 7A, B show TEM images of HeLa cells after the administration of siRNA-BL/MTAB-AuNPs and siRNA-MTAB-AuNPs, respectively (See also Figure S3 in the Supporting Information for an enlarged view and an additional image). In both of cases, AuNPs were predominantly localized within the endocytotic vesicles. We checked the sliced images of 33 different HeLa cells for siRNA-MTAB-AuNPs and found a total of 754 AuNPs within the HeLa cells examined. The numbers are summarized in Table 1. For siRNA-BL/MTAB-AuNPs, 717 AuNPs were counted in images from 20 different

Table 1. Number and Ratio of AuNPs in the Cytosol Determined from TEM Images

	observed total counts	cytosol	ratio of AuNPs in the cytosol (%)
siRNA-MTAB-AuNPs	754[a]	3	0.4
siRNA-BL/MTAB-AuNPs	717[b]	16	2.2

[a]: This number was obtained from sliced images of 33 different cells. [b]: This number was obtained from sliced images of 20 different cells.

cells. Interestingly, 3 and 16 AuNPs were found in the cytosol of the siRNA-MTAB-AuNPs and siRNA-BL/MTAB-AuNPs, respectively. The numbers of AuNPs in the cytosol correspond to 0.4 and 2.2%, respectively, of the total number of AuNP found in the cells. The absolute number of AuNPs located within the cytosol was small; however, that was a 5-fold difference in the ratio between the two complexes. We therefore concluded that the central function of the BLs was to increase the proportion of AuNPs dispersed within the cytosol. At present, we cannot confirm whether the passage to the cytosol is based on endosomal escape or plasma membrane permeation; however, our results (siRNA activity and TEM images) clearly demonstrate that the display of this simple bifurcated ligand on AuNPs plays an important function in the delivery of siRNAs into the cytosol, thus leading to effective gene silencing.

CONCLUSION

In summary, we presented the surface modification of newly synthesized bifurcated ligands having hydrophilic/hydrophobic arms that afford an amphiphilic feature to AuNPs, and demonstrated that the ligand-displaying AuNPs can function as an efficient carrier for the delivery of siRNAs into cytosols. A single BL/MTAB-AuNP with a diameter of 40 nm could be loaded only 26 siRNA molecules. This number was much smaller than that for MTAB-modified cationic AuNPs. Nevertheless, the obvious silencing of the luciferase gene was observed at a concentration ranging from as low as ∼100 pM, whereas the siRNA-MTAB-AuNP conjugate showed little interference. This suggests that BL molecules assist in the permeation of AuNPs from the endocytotic vesicles or plasma membrane to the cytosol because of their high affinity to the membrane, thereby allowing the efficient delivery of the siRNA on the AuNPs to the cytoplasm. Our data will provide useful guidelines for the surface design of various nanoparticles with applications as siRNA delivery carriers.

MATERIALS AND METHODS

Preparation of MTAB-AuNPs. AuNPs stabilized by cetyltrimethylammonium bromide (CTAB) and with a 40 nm of diameter were prepared using a seeding growth method as described previously.[43,44] Briefly, to a seed solution consisting of $HAuCl_4$ (0.01 M, 250 μL) and CTAB (0.1 M, 7.5 mL) was added ice-cold $NaBH_4$ (0.01 M, 600 μL). The resulting seed solution was stirred at room temperature for 2 h. The growth solution was prepared by the sequential addition of CTAB (0.1 M, 2.9 mL), $HAuCl_4$ (0.01 M, 370 μL), and ascorbic acid (0.1 M, 1.8 mL) to water (15 mL). The seed solutions were diluted 10-fold with water. The diluted seed solutions (9.3 μL) were then added to the growth solution. The resultant solutions were mixed by gentle inversion for 10 s and then left undisturbed overnight at 30 °C. CTAB-

stabilized AuNPs were washed by centrifugation (2,000*g* for 10 min) 3 times and the supernatants discarded to remove excess CTAB. MTAB (5 mg) was added to an aqueous solution of washed AuNPs (1 nM, 1 mL). The concentration was estimated by plasmon absorbance at 520 nm using a NanoDrop ND-1000 spectrophotometer (Thermo Fisher, USA). The binding reaction of MTAB to 40 nm AuNPs was performed by the following "heat-and-cool step"; (1) incubation of the AuNP solution for 3 min at 60 °C and then for 2 h at 40 °C (clear solution), (2) cooling on ice for 20 min (MTABs were crystallized), and (3) centrifugation at room temperature and discarding of the supernatant. After repeating this process twice, the solution was incubated at 40 °C for 12 h. Finally, the excess MTAB was removed by centrifugation (2,000*g* for 10 min, three times) and the supernatant discarded. The collected MTAB-AuNPs were redispersed in water, and the final concentration was adjusted to 1 nM.

Preparation of BL/MTAB- and OEG6/MTAB-AuNPs (40 nm in diameter). Using MTAB-AuNPs as a starting material, both BL/MTAB- and OEG6/MTAB-AuNPs were prepared by the addition of a methanol solution of BL or OEG6 (20 uL of 50 mM), respectively, to 1 mL of MTAB-AuNPs solution (1 nM) (final concentration of ligands was approximately 1 mM). These mixtures were incubated for 4 h at room temperature, washed by centrifugation (2,000*g* for 10 min) and the supernatants discarded. The resultant BL/MTAB- and OEG6/MTAB-AuNPs were redispersed in water, and the final concentration was adjusted to 1 nM.

Preparation of BL-AuNPs for NMR Experiment. Citrate coated-AuNPs with a diameter of 15 nm were synthesized according to the previous procedure.[42,43] The synthesized AuNPs were centrifuged (14,100*g* for 20 min) to wash by discarding the supernatants, and they were dispersed with D_2O (ca. 500 nM, 1 mL). A methanol solution of BL (50 mM, 10 μL) was added and incubated for 2 h at 40 °C. To remove the excess BL molecules, the final solution was centrifuged (14 ,100*g* for 20 min), and the supernatant was discarded. Finally, BL-AuNPs were dispersed with 600 μL of D_2O or $CDCl_3$ for NMR measurements.

Preparation of BL-AuNPs and OEG6-AuNPs for Phase-Transfer. Citrate-coated AuNPs with a diameter of 10 nm (9.5 nM, 500 μL) was washed by centrifugation (6,000*g*, 10 min, twice) using an Amicon Ultra 100 K filter and then redispersed in Milli-Q water (ca. 30 nM, 500 μL). A methanol solution of BL or OEG6 (50 mM, 10 μL) was added and sonicated for 10 min, and then incubated for 2 h at 40 °C. This sample was used for the phase-transfer examination without further purification. Chloroform (500 μL) was added to this solution and let stand for 30 min at room temperature. PBS (50 μL) was added to the aqueous phase, vigorously mixed using a Vortex mixer for 30 s and then let stand for overnight.

NMR Analysis of BL-AuNPs Dispersed in D_2O and $CDCl_3$. All NMR measurements for BL-AuNPs were performed on a JEOL ECA600 spectrometer at a proton frequency of 600.17 MHz. The solvent for all AuNPs solutions was replaced with D_2O (Wako Pure Chemical Industries, Japan) or $CDCl_3$ (Wako Pure Chemical Industries, Japan) by centrifugation (14,100*g* for 20 min, twice). The residual water signal was suppressed by presaturation prior to the observation pulse, and relaxation recovery time was set to 2 s. Sample concentration was approximately 500 nM and the number of scans was set to 512.

Determination of the number of siRNAs per AuNPs. To display siRNAs on each type of AuNP (MTAB-, BL/MTAB-, or OEG6/MTAB-AuNPs, 40 nm, 1 nM, 100 μL), ds-siRNA (5 μM, 100 μL) labeled with Alexa-488 was mixed into each AuNP solution, and the solutions were let stand for 3 h at room temperature. Unreacted siRNAs were removed by centrifugation (2,000*g* for 10 min, twice, and 14,000*g* for 3 min). A sodium dodecyl sulfate (SDS) solution (173 mM, 100 μL) was added to the collected AuNPs pellets to release the incorporated siRNAs. The solution was mixed by pipetting and centrifuged (14,100*g* for 3 min) to collect supernatants. Finally, Milli-Q water (100 μL) was added to the collected supernatants and the solutions were subjected to florescent measurements using a NanoDrop 3300 fluorospectrometer (Thermo Fisher, USA) to quantify the released siRNAs.

Knockdown assay using siRNA-AuNP conjugates. The siRNAs for the gene silencing of luciferase used in this study was identical to that used in Henry's report.[48]

Sense strand: 5′-cuuAcGcuGAGuAcuucGAT*T-3′

Antisense strand: 5′-UCGAAGUACUCAGCGUAAGT*T-3′

Lower case letters and asterisks represent 2′-*O*-methyl-nucleotides and phosphorothioate linkages, respectively. This siRNA was kindly provided by Takeda Pharmaceutical Co. Ltd. (Japan). MISSION siRNA Universal Negative Control (Sigma-Aldrich) was used as nontargeted siRNAs. HeLa cells expressing luciferase were cultured in Dulbecco's modified Eagle's medium (DMEM; Sigma-Aldrich) supplemented with 10% fetal bovine serum (FBS; GIBCO BRL, USA) in a white 96-well plate at 37 °C under 5% CO_2 conditions. Culturing was initiated by the seeding of 2,000 cells per well. Medium was replaced after 24 h culture, and then siRNA-AuNPs were added to the medium (final concentration: 15−60 pM). After incubation for 16 h, the medium was refreshed and the cells were then incubated for another 24 h. Intracellular siRNA-AuNP function was tested by the checking the silencing of luciferase expression using a Luciferase Assay System (Promega, USA). A cytotoxicity assay was also performed using CCK-8 (Dojindo Laboratories, Japan). HeLa cells expressing luciferase were kindly provided by Prof. H. Akita of Hokkaido University.

ICP Analysis. To determine the concentration of gold ions incorporated into cells using inductively coupled plasma atomic emission spectroscopy (ICP-AES), we cultured HeLa cells expressing luciferase (2×10^5 cells/well) for 12 h on 6-well plates in DMEM containing 10% FBS at 37 °C under 5% CO_2 conditions. The culture medium was replaced and AuNPs solutions were added at a concentration of 30 pM. Cells cultured for 20 h were washed 3 times in situ with PBS and harvested by trypsin treatment. Aqua regia (1 mL) was added to the collected cell pellets and the solutions were incubated for 1 day to achieve complete ionization of the gold. The solutions were diluted with 10 mL of Milli-Q water and subjected to ICP analysis. The concentration of gold ions measured with ICP was converted to the number of gold particles as described previously.[49]

TEM analyses. HeLa cells were cultured with the siRNA-associated AuNPs (final concentration: 30 pM) for 3 h in DMEM on BioCoat poly-D-lysine 8-well CultureSlides (BD). Cells were washed 3 times with PBS and fixed in 2.5% glutaraldehyde dissolved in 0.1 M phosphate buffer (pH 7.4) by incubation overnight at 4 °C. Subsequently, an aqueous solution of 1% osmium tetroxide and 1.5% potassium ferrocyanide were applied to the fixed cells for 2 h at room temperature, and the cells were dehydrated in a graded ethanol series. Finally, the fixed cells were embedded in Epon 812 (TAAB). Ultrathin sections were then cut on a RMC Ultramicrotome MTX. The sections were stained with uranyl acetate followed by lead citrate and examined at 80 kV with a JEM-1400 transmission electron microscope (TEM; JEOL, Japan).

■ ASSOCIATED CONTENT

Ⓢ Supporting Information

^{1}H NMR spectrum of BL, enlarged TEM image of HeLa cell. This material is available free of charge via the Internet at http://pubs.acs.org/.

■ AUTHOR INFORMATION

Corresponding Authors

*E-mail: kniikura@poly.es.hokudai.ac.jp.

*E-mail: ijiro@poly.es.hokudai.ac.jp.

Author Contributions

†K.N. and K.K.contributed equally.

Notes

The authors declare no competing financial interest.

■ ACKNOWLEDGMENTS

The authors thank Ms. K. Otsuki, Mr. M. Usui, and Ms. A. Abe of the Mass spectrometry Service (RIKEN) for MALDI-TOFMS analysis.

■ REFERENCES

(1) Haasnoot, J.; Westerhout, E. M.; Berkhout, B. RNA Interference against Viruses: Strike and Counterstrike. *Nat. Biotechnol.* **2007**, *25*, 1435−1443.
(2) Devi, G. R. siRNA-Based Approaches in Cancer Therapy. *Cancer Gene Ther.* **2006**, *13*, 819−829.
(3) Behlke, M. A. Progress Towards in Vivo Use of siRNAs. *Mol. Ther.* **2006**, *13*, 644−670.
(4) Li, C. X.; Parker, A.; Menocal, E.; Xiang, S.; Borodynaansky, L.; Fruehauf, J. H. Delivery of RNA Interference. *Cell Cycle* **2006**, *15*, 2103−2109.
(5) Castanotto, D.; Rossi, J. J. The Promises and Pitfalls of RNA-Interference-Based Therapeutics. *Nature* **2009**, *457*, 426−433.
(6) Dorsett, Y.; Tuschl, T. Applications in Functional Genomics and Potential as Therapeutics. *Nat. Rev. Drug Discovery* **2004**, *3*, 318−329.
(7) Davis, M. E. The First Targeted Delivery of siRNA in Humans via a Self-Assembling, Cyclodextrin Polymer-Based Nanoparticle: From Concept to Clinic. *Mol. Pharmaceutics* **2009**, *6*, 659−668.
(8) Shim, M. S.; Kwon, Y. J. Efficient and Targeted Delivery of siRNA in Vivo. *FEBS J.* **2010**, *277*, 4814−4827.
(9) Tan, S. J.; Kiatwuthinon, P.; Roh, Y. H.; Kahn, J. S.; Luo, D. Engineering Nanocarriers for siRNA Delivery. *Small* **2011**, *7*, 841−856.
(10) Lytton-Jean, A. K. R.; Langer, R.; Anderson, D. G. Five Years of siRNA Delivery: Spotlight on Gold Nanoparticles. *Small* **2011**, *7*, 1932−1937.
(11) Fratila, R. M.; Mitchell, S. G.; del Pino, P.; Grazu, V.; de la Fuente, J. M. Strategies for the Biofunctionalization of Gold and Iron Oxide Nanoparticles *Langmuir* Article ASAP, DOI: 10.1021/la5015658.
(12) Kim, S. T.; Chompoosor, A.; Yeh, Y.-C.; Agasti, S. S.; Solfiell, D. J.; Rotello, V. M. Dendronized Gold Nanoparticles for siRNA Delivery. *Small* **2012**, *8*, 3253−3256.
(13) Song, W.-J.; Du, J.-Z.; Sun, T.-M.; Zhang, P.-Z.; Wang, J. Gold Nanoparticles Capped with Polyethyleneimine for Enhanced siRNA Delivery. *Small* **2010**, *6*, 239−246.
(14) Conde, J.; Ambrosone, A.; Sanz, V.; Hernandez, Y.; Marchesano, V.; Tian, F.; Child, H.; Berry, C. C.; Ibarra, M. R.; Baptista, P. V.; Tortiglione, C.; de la Fuente, J. M. Design of Multifunctional Gold Nanoparticles for In Vitro and In Vivo Gene Silencing. *ACS Nano* **2012**, *6*, 8316−8324.
(15) Thakor, A. S.; Jokerst, J.; Zavaleta, C.; Massoud, T. F.; Gambhir, S. S. Gold Nanoparticles: A Revival in Precious Metal Administration to Patients. *Nano Lett.* **2011**, *11*, 4029−4036.
(16) Personick, M. L.; Mirkin, C. A. Making Sense of the Mayhem behind Shape Control in the Synthesis of Gold Nanoparticles. *J. Am. Chem. Soc.* **2013**, *135*, 18238−18247.
(17) Oishi, M.; Nakaogami, J.; Ishii, T.; Nagasaki, Y. Smart PEGylated Gold Nanoparticles for the Cytoplasmic Delivery of siRNA to Induce Enhanced Gene Silencing. *Chem. Lett.* **2006**, *35*, 1046−1047.
(18) Giljohann, D. A.; Seferos, D. S.; Prigodich, A. E.; Patel, P. C.; Mirkin, C. A. Gene Regulation with Polyvalent siRNA-Nanoparticle Conjugates. *J. Am. Chem. Soc.* **2009**, *131*, 2072−2073.
(19) Singh, N.; Agrawal, A.; Leung, A. K. L.; Sharp, P. A.; Bhatia, S. N. Effect of Nanoparticle Conjugation on Gene Silencing by RNA Interference. *J. Am. Chem. Soc.* **2010**, *132*, 8241−8243.
(20) Caruso, F. Nanoengineering of Particle Surfaces. *Adv. Mater.* **2001**, *13*, 11−22.
(21) Wang, Y.; Angelatos, A. S.; Caruso, F. Template Synthesis of Nanostructured Materials via Layer-by-Layer Assembly. *Chem. Mater.* **2008**, *20*, 848−858.
(22) Elbakry, A.; Zaky, A.; Liebl, R.; Rachel, R.; Goepferich, A.; Breunig, M. Layer-by-Layer Assembled Gold Nanoparticles for siRNA Delivery. *Nano Lett.* **2009**, *9*, 2059−2064.
(23) Kim, S. T.; Saha, K.; Kim, C.; Rotello, V. M. The Role of Surface Functionality in Determining Nanoparticle Cytotoxicity. *Acc. Chem. Res.* **2013**, *46*, 681−691.
(24) Wang, T.; Bai, J.; Jiang, X.; Nienhaus, G. U. Cellular Uptake of Nanoparticles by Membrane Penetration: A Study Combining Confocal Microscopy with FTIR Spectroelectrochemistry. *ACS Nano* **2012**, *6*, 1251−1259.
(25) Nel, A. E.; Mädler, L.; Velegol, D.; Xia, T.; Hoek, E. M. V.; Somasudaran, P.; Klaessg, F.; Castranova, V.; Thompson, M. Understanding Biophysicochemical Interactions at the Nano−Bio Interface. *Nat. Mater.* **2009**, *8*, 543−557.
(26) Lin, J.; Zhang, H.; Chen, Z.; Zheng, Y. Penetration of Lipid Membranes by Gold Nanoparticles: Insights into Cellular Uptake, Cytotoxicity, and Their Relationship. *ACS Nano* **2010**, *4*, 5421−5429.
(27) Dubavik, A.; Lesnyak, V.; Thiessen, W.; Gaponik, N.; Wolff, T.; Eychmüller, A. Synthesis of Amphiphilic CdTe Nanocrystals. *J. Phys. Chem. C* **2009**, *113*, 4748−4750.
(28) Dubavik, A.; Sezgin, E.; Lesnyak, V.; Gaponik, N.; Schwille, P.; Eychmüller, A. Penetration of Amphiphilic Quantum Dots through Model and Cellular Plasma Membranes. *ACS Nano* **2012**, *6*, 2150−2156.
(29) Sekiguchi, S.; Niikura, K.; Matsuo, Y.; Ijiro, K. Hydrophilic Gold Nanoparticles Adaptable for Hydrophobic Solvents. *Langmuir* **2012**, *28*, 5503−5507.
(30) Kobayashi, K.; Niikura, K.; Takeuchi, C.; Sekiguchi, S.; Ninomiya, T.; Hagiwara, K.; Mitomo, H.; Ito, Y.; Osada, Y.; Ijiro, K. Enhanced Cellular Uptake of Amphiphilic Gold Nanoparticles with Ester Functionality. *Chem. Commun.* **2014**, *50*, 1265−1267.
(31) Verma, A.; Uzun, O.; Hu, Y.; Hu, Y.; Han, H.-S.; Watson, N.; Chen, S.; Irvine, D. J.; Stellacci, F. Surface-Structure-Regulated Cell-Membrane Penetration by Monolayer- Protected Nanoparticles. *Nat. Mater.* **2008**, *7*, 588−595.
(32) Zubarev, E. R.; Xu, J.; Sayyad, A.; Gibson, J. D. Amphiphilic Gold Nanoparticles with V-Shaped Arms. *J. Am. Chem. Soc.* **2006**, *128*, 4958−4959.
(33) Boussif, O.; Lezoualc'h, F.; Zanta, M. A.; Mergny, M. D.; Scherman, D.; Demeneix, B.; Behr, J.-P. A Versatile Vector for Gene and Oligonucleotide Transfer into Cells in Culture and *in vivo*: Polyethyleimene. *Proc. Natl. Acad. Sci. U.S.A.* **1995**, *92*, 7297−7301.
(34) Bayles, A. R.; Chahal, H. S.; Chahal, D. S.; Goldbeck, C. P.; Cohen, B. E.; Helms, B. A. Rapid Cytosolic Delivery of Luminescent Nanocrystals in Live Cells with Endosome- Disrupting Polymer Colloids. *Nano Lett.* **2010**, *10*, 4086−4092.
(35) Evans, C. W.; Fitzgerald, M.; Clemons, T. D.; House, M. J.; Padman, B. S.; Shaw, J. A.; Saunders, M.; Harvey, A. R.; Zdyrko, B.; Luzinov, I.; Silva, G. A.; Dunlop, S. A.; Iyer, K. S. Multimodal Analysis of PEI-Mediated Endocytosis of Nanoparticles in Neural Cells. *ACS Nano* **2011**, *5*, 8640−8648.
(36) Dykman, L. A.; Khlebtsov, N. G. Uptake of Engineered Gold Nanoparticles into Mammalian Cells. *Chem. Rev.* **2014**, *114*, 1258−1288.
(37) Futaki, S.; Suzuki, T.; Ohashi, W.; Yagami, T.; Tanaka, S.; Ueda, K.; Sugiura, Y. Arginine-rich Peptides. *J. Biol. Chem.* **2001**, *276*, 5836−5840.
(38) Vigderman, L.; Manna, P.; Zubarev, E. R. Quantitative Replacement of Cetyl Trimethylammonium Bromide by Cationic Thiol Ligands on the Surface of Gold Nanorods and Their Extremely Large Uptake by Cancer Cells. *Angew. Chem., Int. Ed.* **2012**, *51*, 636−641.
(39) Kim, H.; Carney, R. P.; Reguera, J.; Ong, Q. K.; Liu, X.; Stellacci, F. Synthesis and Characterization of Janus Gold Nanoparticles. *Adv. Mater.* **2012**, *24*, 3857−3863.
(40) Liu, X.; Yu, M.; Kim, H.; Mameli, M.; Stellacci, F. Determination of Monolayer- Protected Goldnanoparticle Ligand−Shell Morphology Using NMR. *Nat. Commun.* **2012**, No. 1182.

(41) Chithrani, B. D.; Ghazani, A. A.; Chan, W. C. W. Determining the Size and Shape Dependence of Gold Nanoparticle Uptake into Mammalian Cells. *Nano Lett.* **2006**, *6*, 662−668.
(42) Sau, T. K.; Murphy, C. J. Room Temperature, High-Yield Synthesis of Multiple Shapes of Gold Nanoparticles in Aqueous Solution. *J. Am. Chem. Soc.* **2004**, *126*, 8648−8649.
(43) Chen, H.; Kou, X.; Yang, Z.; Ni, W. Shape- and Size-Dependent Refractive Index Sensitivity of Gold Nanoparticles. *Langmuir* **2008**, *24*, 5233−5237.
(44) Baun, G. B.; Pallaoro, A.; Wu, G.; Missirilis, D.; Zasadzinski, J. A.; Tirrell, M.; Reich, N. O. Laser-Activated Gene Silencing *via* Gold Nanoshell-siRNA Conugates. *ACS Nano* **2009**, *3*, 2007−2015.
(45) Wang, Y.; Huang, L. A "Window onto siRNA Delivery. *Nat. Biotechnol.* **2013**, *31*, 611−612.
(46) Gilleron, J.; Querbes, W.; Zeigerer, A.; Borodovsky, A.; Marsico, G.; Schubert, U.; Manygoats, K.; Seifert, S.; Andree, C.; Stöter, M.; Epstein-Barash, H.; Zhang, L.; Koteliansky, V.; Fitzgeranld, K.; Faval, E.; Bickle, M.; Kalaidzidis, Y.; Akinc, A.; Maier, M.; Zerial, M. Image-Based Analysis of Lipid Nanoparticle−Mediated siRNA Delivery, Intracellular Trafficking and Endosomal Escape. *Nat. Biotechnol.* **2013**, *31*, 638−646.
(47) Sahay, G.; Querbes, W.; Alabi, C.; Eltoukhy, A.; Sarkar, S.; Zurenko, C.; Karagiannis, E.; Love, K.; Chen, D.; Zoucu, R.; Buganim, Y.; Schroeder, A.; Langer, R.; Anderson, D. G. Efficiency of siRNA Delivery by Lipid Nanoparticles is Limited by Endocytic Recycling. *Nat. Biotechnol.* **2013**, *31*, 653−658.
(48) Svensson, R. U.; Shey, M. R.; Ballas, Z. K.; Dorkin, J. R.; Goldberg, M.; Akinc, A.; Langer, R.; Anderson, D. G.; Bumcrot, D.; Henry, M. D. Assessing siRNA Pharmacodynamics in a Luciferase-Expressing Mouse. *Mol. Ther.* **2008**, *16*, 1995−2001.
(49) Oh, E.; Delehanty, J. B.; Sapsford, K. E.; Susumu, K.; Goswami, R.; Blanco-Canosa, J. B.; Dawson, P. E.; Granek, J.; Shoff, M.; Zhang, Q.; Goering, P. L.; Huston, A.; Medintz, I. L. Cellular Uptake and Fate of PEGylated Gold Nanoparticles Is Dependent on Both Cell-Penetration Peptides and Particle Size. *ACS Nano* **2011**, *5*, 6434−6448.